ACS APPLIED NANO MATERIALS

www.acsanm.org Article

Hollow Ruthenium Nanoparticles with Enhanced Catalytic Activity for Colorimetric Detection of C-Reactive Protein

Seong Eun Son, Pramod K. Gupta, Won Hur, Han Been Lee, Do Kyoung Han, and Gi Hun Seong*

Cite This: *ACS Appl. Nano Mater.* 2023, 6, 11435−11442 Read Online

ACCESS | Metrics & More | Article Recommendations | Supporting Information

ABSTRACT: Hollow structures can improve the physical and chemical characteristics of nanoparticles. In the present work, we synthesized hollow ruthenium nanoparticles (HRNs) using a galvanic replacement reaction. Compared to normal nanoparticles, the hollow structures had greater surface area, leading to enhanced transport of reactants. Transmission electron microscopy images revealed the formation of distinct hollow structures with an average size of 30 nm. As a peroxidase mimic, the HRNs showed excellent catalytic activity for the oxidation of 3,3′,5,5′-tetramethylbenzidine due to the increased surface area of the hollow structure. Moreover, the catalytic efficiency of the HRNs was greater than that of horseradish peroxidase, due to the presence of hollow structures. The HRNs were applied to the colorimetric detection of C-reactive protein (CRP) by enzyme-linked immunosorbent assay (ELISA). The results displayed great sensitivity for CRP levels of 0.12−7.8 ng/mL and a limit of detection of 33.2 pg/mL. In the recovery test, the assay showed accurate detection of CRP in spiked human serum with recovery values of 97.0−98.0%. The results of the present study reveal the validity and possibility of HRNs as alternatives to natural enzymes for application to conventional ELISA.

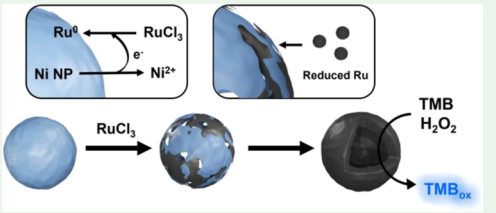

KEYWORDS: *hollow nanoparticles, galvanic replacement, noble metal, nanozymes, peroxidase mimic*

INTRODUCTION

Nanozymes, which are artificial nanomaterials with enzyme-mimicking activities, have been studied for decades. As substitutes for natural enzymes, nanozymes possess several advantages including low cost, simple preparation, high stability, and remarkable catalytic activity.[1] After discovery of the enzyme-like activity of magnetite nanoparticles,[2] a variety of nanomaterials, including metal oxides,[3,4] metal organic frameworks,[5] noble metals,[6−9] and carbon-based nanomaterials,[10] have been developed as nanozymes. Of these nanozymes, noble metal-based nanomaterials have received significant attention due to their biocompatibility, high chemical stability, and suitability for surface modification.[11,12] To date, nanomaterials developed with several combinations of noble metals have shown excellent catalytic activity.[13,14] Even though noble metal-based nanomaterials have displayed great activity, it is challenging to control their surface properties, size, and morphology for enhanced catalytic activity.[15−17]

In recent years, the development of hollow structures has been studied as a strategy to control the morphology and surface properties of nanomaterials. The hollow structures, which consist of distinct shell layers and an inner cavity, offer several advantages, such as increased surface to volume ratio, facile transport of reactants, and high stability.[18,19] Furthermore, the high surface area of the hollow structure allows abundant exposure of active sites, resulting in enhanced chemical properties.[20] Hollow nanomaterials usually are synthesized by chemical etching,[21,22] degradation of a bio-organic molecule template,[23,24] or a galvanic replacement reaction (GRR).[25,26] Of these methods, GRR is most commonly used to fabricate hollow nanomaterials due to its numerous advantages including simplicity, high tunability, and short reaction time.[27,28] In a GRR, the metal precursor, which has a high reduction potential, is reduced by sacrificing a template with a low reduction potential. Recently, a variety of hollow noble metal nanomaterials have been synthesized using a GRR. These nanomaterials displayed enhanced catalytic activity in several applications, such as oxygen reduction reactions,[29] antioxidant screening,[30] and biomarker detection.[31] However, there have been few reports of the application of hollow nanomaterials as enzyme-mimetic nanozymes.

Herein, we fabricated hollow ruthenium nanoparticles (HRNs) using a simple GRR method in which nickel nanoparticles were used as a sacrificial template. As far as we know, there have been no reports of the generation of HRNs by a GRR. The HRNs displayed excellent peroxidase-mimetic activity which catalyzed the reaction of 3,3′,5,5′-tetramethylbenzidine (TMB) with hydrogen peroxide (H_2O_2). Furthermore, the catalytic efficiency of the HRNs toward TMB and

Received: April 4, 2023
Accepted: June 23, 2023
Published: July 5, 2023

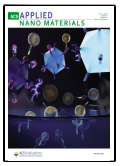

https://doi.org/10.1021/acsanm.3c01414
ACS Appl. Nano Mater. 2023, 6, 11435−11442

H_2O_2 was greater than that of horseradish peroxidase (HRP). The impressive catalytic activity of the HRNs was attributed to the hollow structure, which resulted in increased surface area and active sites. The HRNs were used as a detection probe in conventional enzyme-linked immunosorbent assay (ELISA) for C-reactive protein (CRP), which is a key indicator of cardiovascular disease and inflammation. HRN-based ELISA showed great linearity for CRP. These results demonstrate the potential applicability of HRNs as alternatives to natural enzymes in the field of biosensing.

EXPERIMENTAL SECTION

Materials. Nickel chloride hydrate ($NiCl_2{\cdot}xH_2O$), ruthenium chloride hydrate ($RuCl_3{\cdot}xH_2O$), citric acid, terephthalic acid (TA), *N*-(3-dimethylaminopropyl)-*N*′-ethylcarbodiimide hydrochloride (EDC), *N*-hydroxysulfosuccinimide (Sulfo-NHS), hydrogen peroxide (H_2O_2), TMB, Nafion solution, bovine serum albumin (BSA), glucose (Glu), creatinine (CT), urea, ascorbic acid (AA), uric acid (UA), cholesterol (Cho), γ-globulin (Glb), HRP, human serum albumin (HSA), superoxide dismutase (SOD), ethylenediaminetetraacetic acid (EDTA), and dimethyl sulfoxide (DMSO) were obtained from Sigma-Aldrich (St. Louis, MO, USA). Sulfuric acid (H_2SO_4, 98%) was obtained from Daejung Co., Ltd. (Siheung, South Korea). 2 M Phosphate-buffered saline (PBS, pH 7.4) was supplied from Biosesang Co., Ltd. (Seongnam, South Korea). Sodium borohydride ($NaBH_4$) was obtained from Alfa Aesar (Ward Hill, MA, USA). Acetic acid (HAc) was purchased from Junsei Chemical Co., Ltd. (Tokyo, Japan). Indium tin oxide (ITO) glass was obtained from Samsung Corning Advanced Glass (Asan, South Korea). Mouse anti-CRP monoclonal capture and detection antibodies (cAb-CRP and dAb-CRP, respectively) were supplied by Fitzgerald Industries International (Acton, MA, USA). HRP-conjugated anti-CRP antibody was purchased from Abcam Inc. (Cambridge, U.K.).

Synthesis of HRNs. The HRNs were prepared by a simple one-pot chemical synthesis. First, 0.15 mmol of $NiCl_2$ and 0.05 mmol of citric acid were added to 100 mL of deionized water and sonicated. Then, 0.5 mL of $NaBH_4$ (1 M) was added. The solution color changed from transparent to dark brown, indicating the production of Ni nanoparticles (Ni NPs). After 15 min of incubation, 1 mL of $RuCl_3$ solution (40 mM) containing 0.05 mmol of citric acid was added via 20 additions of 50 μL at 30 s intervals. At this point, a GRR occurred in which the Ru salt consumed the Ni NPs due to the differences of reduction potential of Ru and Ni. After incubation for 3 h, the solution was washed through centrifugation (15,000 rpm, 20 min) three times with deionized water. The obtained HRNs were redispersed in 20 mL of deionized water and stored at 4 °C until use.

Enzyme-Mimicking Activity. To evaluate the enzyme-mimetic activity of the HRNs, the absorbance of TMB was monitored in the presence and absence of H_2O_2. Then, TMB and H_2O_2 were added to 0.17 μg/mL of HRNs dissolved in 0.1 M HAc−NaAc buffer (pH 5.5), and the absorbance spectrum of the solution was recorded. In addition, the time-dependent absorbance was measured to calculate the Michaelis constant (K_m), maximum reaction rate (V_{max}), and turnover number (K_{cat}). The K_m and V_{max} were obtained using the Michaelis−Menten and double reciprocal equations. The equations are described in the Supplementary Information.

Catalytic Mechanism of the HRNs. The generation of free radicals from H_2O_2 by HRNs was investigated. First, the generation of hydroxyl radical (•OH) was evaluated using TA. Briefly, 0.4 mM TA, 20 mM H_2O_2, and 3.5 μg/mL HRNs were mixed. After 1 h incubation, the fluorescence of TA was measured. In addition, DMSO was employed as a scavenger of •OH. To further investigate the generation of other free radicals, the absorbance of oxidized TMB (TMB_{ox}) was observed in the presence of scavengers. For the reaction, a solution containing 0.6 mM TMB, 20 mM H_2O_2, and 0.6 μg/mL HRNs was mixed with free radical scavengers (DMSO, SOD, and EDTA). After 1 min incubation, the absorbance was measured.

Cyclic voltammetry (CV) and chronoamperometry (CA) were conducted to investigate the accelerated electron transfer between substrates by HRN. As a working electrode, the ITO glass was modified with Nafion and HRN. Briefly, a casting mixture containing 50 μg/mL HRN and 0.5% Nafion was prepared. Then, 15 μL of the mixture was drop-casted on the ITO glass and dried. Finally, the modified electrode (Nafion/HRN/ITO) was washed with water and dried. Ag/AgCl (saturated in 3 M NaCl) and platinum wire were used as reference and counter electrodes, respectively. In the CV experiment, all the electrodes were immersed in 5 mL of 10 mM PBS. Then, the current was monitored at a potential range of −1.0 to 0 V. In the CA, the current response was measured by adding 50 μL of 1 M H_2O_2 to the 5 mL PBS solution every 50 s.

Conjugation of dAb-CRP onto the HRNs. To prepare the dAb-CRP conjugated HRNs (dAb-HRNs), 1 mL of a 65 μg/mL solution of HRNs was mixed with 5 μL of 25 mM EDC and 5 μL of 25 mM Sulfo-NHS. After 1 h of incubation, the solution was washed twice with water and resuspended in 1 mL of water. Then, 10 μL of 1 mg/mL dAb-CRP was added. The solution was incubated for 4 h at 4 °C after which 110 μL of 3% BSA was added. After 1 h of incubation at room temperature, the dAb-HRNs were washed twice with water. Then, the dAb-HRNs were resuspended in 0.5 mL of 10 mM PBS containing 0.3% BSA at 4 °C for later use.

CRP Detection by ELISA. The CRP concentration was analyzed by sandwich ELISA in a microplate. First, the microplates were treated with 100 μL of cAb-CRP (5 μg/mL) and incubated at 4 °C, overnight. After washing the microplate with 10 mM PBS containing 0.05% Tween 20 (PBST), 200 μL of 2% BSA was added and incubated for 3 h at room temperature. The microplate was washed three times using PBST and stored in a refrigerator. In the sandwich ELISA, 100 μL of CRP (0−7.8 ng/mL) was added to a cAb-CRP-treated microplate. The microplate was sealed and incubated for 2 h at 37 °C. The microplate was washed with PBST three times, and 100 uL of dAb-HRN (1.3 μg/mL) was added. The microplate was incubated for 1 h at 37 °C and washed with PBST five times. Next, 100 uL of a substrate solution of 0.6 mM TMB and 50 mM H_2O_2 in 0.1 M HAc-NaAc buffer (pH 5.5) was added. The solution was incubated for 5 min at room temperature. Finally, 50 μL of stop solution (0.5 M H_2SO_4) was added. At this point, the color of the TMB changed from blue to yellow, indicating that the reaction was complete. Finally, the absorbance was measured at a wavelength of 450 nm.

For HRP-based ELISA, the procedures for the incubation of CRP and HRP anti-CRP antibody (0.5 μg/mL) were the same as in HRN-based ELISA. In the final step, 100 μL of 0.1 M HAc-NaAc buffer (pH 5.5) including 0.5 mM TMB and 5 mM H_2O_2 was added and incubated for 20 min. After incubation, 50 μL of H_2SO_4 was added, and the absorbance was measured.

Characterization. The morphology of the HRNs was confirmed by transmission electron microscopy (TEM, JEOL JEM-2010, USA). The crystalline structure was investigated by X-ray diffractometry (XRD, D/MAX-2500, Rigaku, USA). The elemental composition of the HRNs was evaluated by X-ray photoelectron spectroscopy (XPS, K-ALPHA, Thermo Fisher Scientific Inc., U.K.). The absorbance spectra were measured with a UV−visible spectrometer (OPTIZEN 2120UV, Mecasys Co. Ltd., South Korea). The absorbance of the reaction on the microplate was recorded with a multimode microplate reader (BioTek instrument Inc., USA).

RESULTS AND DISCUSSION

Characterization of HRNs. The HRNs used in the present study were fabricated by a GRR-based synthesis (Figure 1). $NiCl_2$ was reduced by the addition of $NaBH_4$, resulting in Ni NPs. Then, the addition of $RuCl_3$ caused a GRR with the Ni NPs due to the difference of reduction potential between Ru and Ni. The Ru ion, which has a higher reduction potential (+0.60 V) than Ni (−0.24 V),[32] was reduced to metallic Ru nanoparticles and covered the surface of the Ni NPs. At this

https://doi.org/10.1021/acsanm.3c01414
ACS Appl. Nano Mater. 2023, 6, 11435−11442

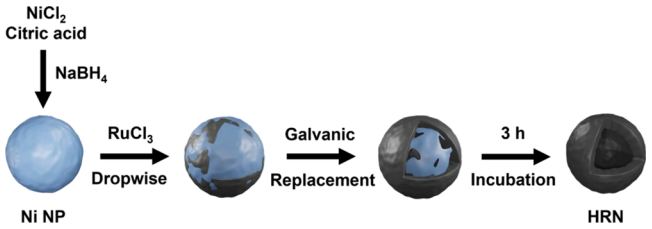

Figure 1. Schematic illustration of the synthesis of HRNs by a GRR.

point, the Ni NPs, which were a sacrificial template, were gradually consumed, resulting in a hollow structure.

The morphology and size of the HRNs were investigated with TEM. As shown in Figure 2A, the HRNs had a well-dispersed hollow structure with distinct shell layers and an internal cavity. Furthermore, the HRNs exhibited a uniform size distribution with an average diameter of 30 nm (inset of Figure 2A). This narrow size distribution could be attributed to the presence of citric acid, which was employed as a stabilizing agent.[12] The thickness of the shell layers was ~4 nm (Figure 2B). To further study HRN formation by GRR, TEM images of the HRNs were captured at different incubation times (Figure S1). First, amorphous Ni NPs with a diameter of 25 nm were synthesized (Figure S1A). After the addition of $RuCl_3$, nanoparticles were produced on the surface of the Ni NPs, suggesting the generation of Ru seeds (Figure S1B). As the reaction proceeded, more $RuCl_3$ was reduced to Ru nanoparticles by a GRR, resulting in a Ru layer. At this point, the Ni NPs gradually oxidized and disassembled (Figures S1C,D). After 3 h of incubation, the contrast between the Ru layer and the Ni core became clear (Figure S1E). This result indicated that the GRR occurred between $RuCl_3$ and the Ni NPs. The high-resolution (HR) TEM image in Figure 2C shows lattice spacings of 0.21 and 0.24 nm, corresponding to the (101) and (100) planes of the HRNs, respectively. Furthermore, the crystallinity of the HRNs was investigated by XRD (Figure S2). The XRD result showed four distinct peaks that corresponded to the (100), (101), (102), and (110) planes, indicating a hexagonal close-packed structure. The Ru/Ni molar ratio of the HRNs obtained by inductively coupled plasma atomic emission spectroscopy (ICP-AES) was 85:15, which corresponded to the results of energy-dispersive X-ray spectroscopy (EDX) (Figure 2D). Compared to the initial feed ratio of Ru/Ni (20:80), the molar ratio of HRNs was significantly changed, demonstrating that a GRR occurred in the synthesis.

The elemental composition of the HRNs was confirmed using XPS (Figure 3). The survey spectra showed the distinct

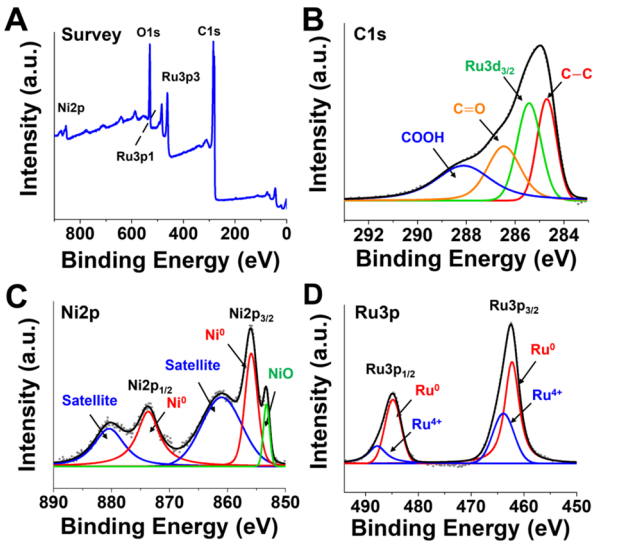

Figure 3. (A) XPS spectra of HRNs. HR-XPS spectra of (B) C 1s, (C) Ni 2p, and (D) Ru 3p.

peaks of the HRNs (Figure 3A). The Ru 3p1 and Ru 3p3 peaks were observed at 450−500 eV. The peaks for C 1s and O 1 s were observed near 285 and 530 eV, respectively. The small peak around 800 to 850 eV corresponded to Ni 2p, suggesting that a small amount of Ni remained after the GRR. In addition, the HR-XPS spectrum for each element was investigated.

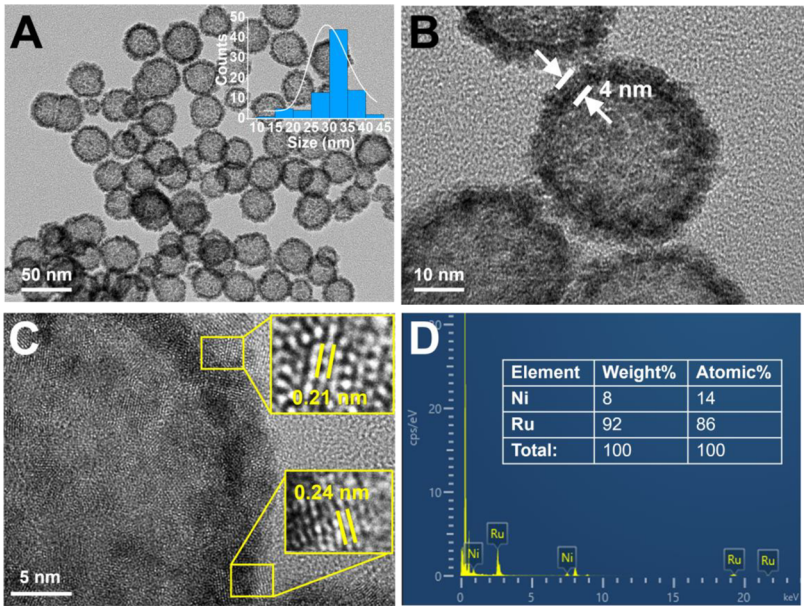

Figure 2. (A,B) TEM images of the HRNs. Inset shows the size distribution. (C) HR-TEM image. (D) EDX results.

https://doi.org/10.1021/acsanm.3c01414
ACS Appl. Nano Mater. 2023, 6, 11435−11442

Figure 3B shows the HR-XPS spectrum of C 1s. The deconvoluted C 1s spectrum showed three distinct peaks at 288.1, 286.5, and 284.7 eV, corresponding to COOH, C═O, and C−C, respectively. This observation revealed the presence of citric acid on the surface of the HRNs. Among these functional ligands, the −COOH group is activated by EDC/NHS for antibody conjugation. The spectrum also contained another peak at 285.4 eV, which corresponded to Ru $3d_{3/2}$. The deconvoluted spectrum for Ni 2p displayed two peaks at 871.3 (Ni $2p_{1/2}$) and 853.5 eV (Ni $2p_{3/2}$), corresponding to metallic Ni (Ni^0) (Figure 3C). The additional two peaks at 878.0 and 858.7 eV were satellite peaks.[33] In addition to these, another peak was observed at ∼851.0 eV, indicative of the NiO species. Figure 3D shows the deconvolution of the Ru 3p spectrum. The spectrum showed two doublet peaks at 484.8 (Ru $3p_{1/2}$) and 462.2 eV (Ru $3p_{3/2}$), which indicated metallic Ru (Ru^0). Another two peaks at ∼487.8 and 463.9 eV revealed Ru^{4+}, produced by the inevitable exposure of the sample to air. The elemental ratio (at%) of Ru/Ni in the HRNs was 84:16, which further supported the ICP-AES and EDX results.

Enzyme-like Activity of the HRNs. Figure 4A displays the UV−vis absorbance of TMB with different compositions.

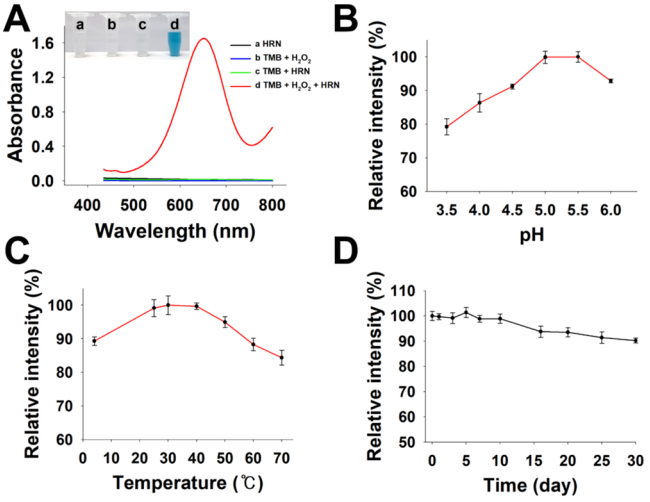

Figure 4. (A) UV−vis spectra of TMB with different compositions. Inset indicates the corresponding optical image. Effects of (B) pH and (C) temperature on peroxidase-like activity of the HRNs. (D) Long-term storage stability of the HRNs for 1 month.

In the presence of H_2O_2, the TMB was quickly oxidized to a blue-colored product, TMB_{ox}, which demonstrated the great peroxidase-like activity of the HRNs. In the absence of H_2O_2, the absorbance of TMB_{ox} was negligible, indicating very weak oxidase-like activity. Furthermore, the peroxidase-like activity of the HRN was compared with Ni NPs and Ru NPs (Figure S3). The catalytic activity of the HRN was significantly greater than that of Ni NPs and Ru NPs, indicating the enhanced chemical properties of HRN due to the presence of a hollow structure. Then, the effects of pH and temperature on the enzyme-like activity of the HRNs were evaluated. As shown in Figure 4B, the maximum activity of the HRNs was observed at pH 5.5. The decrease in catalytic activity at higher pH was due to the instability of H_2O_2 and weak solubility of TMB.[12] Furthermore, the variations of hydration shell formation on the surface of the HRNs resulted in an activity decrease under acidic conditions.[34,35] In terms of temperature, the maximum activity of the HRNs was observed from 25 to 40 °C. Above 40 °C, the activity gradually decreased due to the decomposition of H_2O_2. The long-term stability of the HRNs demonstrated approximately 90% of their catalytic activity for one month, suggesting good stability (Figure 4D). From these results, further experiments were conducted at a pH of 5.5 and room temperature.

Kinetic Assay of HRNs. The catalytic efficiency of the HRNs was evaluated by calculating the kinetic parameters toward TMB and H_2O_2. First, the initial velocity (V_0) against the substrate concentrations ([S]) was plotted, showing typical Michaelis−Menten curves (Figure 5A,B). The V_0 was

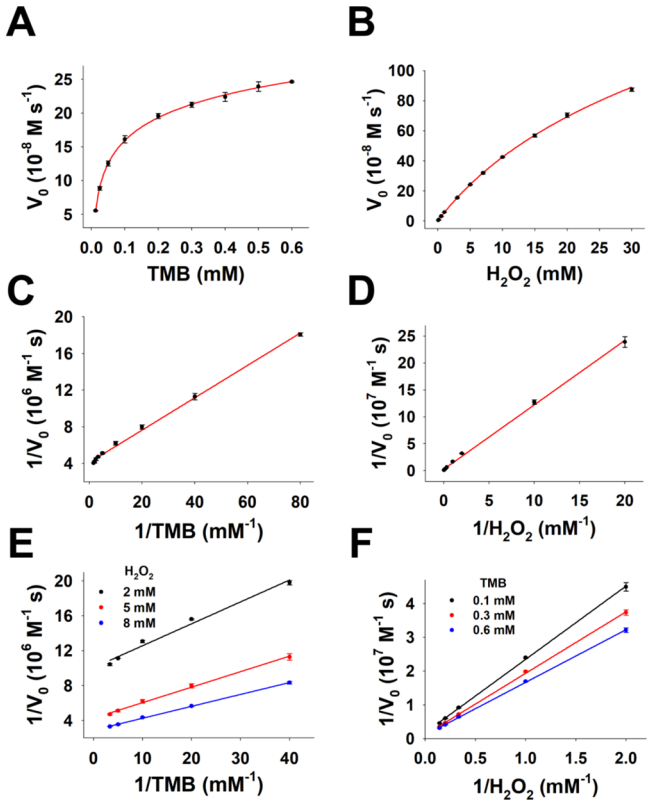

Figure 5. Kinetic assays of the HRNs. (A,B) Michaelis−Menten and (C,D) Lineweaver-Burk plots for TMB and H_2O_2. Concentrations of HRNs, TMB, and H_2O_2 were fixed at 2.45 pM, 0.60 mM, and 5.0 mM, respectively. (E,F) Lineweaver−Burk plots for different substrate concentrations.

calculated from S/ε, where S represents the initial slope value in a time-dependent absorbance curve and ε refers to the molar extinction coefficient of TMB at 652 nm wavelength (39,000 M^{-1} cm^{-1}). Subsequently, the Lineweaver−Burk plots were obtained by taking reciprocal of Michaelis−Menten curves (Figure 5C,D). The K_m, V_{max}, and K_{cat} were obtained using Lineweaver−Burk plots and the corresponding equations. K_m describes the affinity of an enzyme toward a substrate: the lower the K_m, the higher the affinity of the enzyme. K_{cat} represents the number of substrates transformed per unit time by a single enzyme. Thus, a higher K_{cat} value indicates a higher catalytic efficacy. Table 1 shows the kinetic parameters of the HRNs, other ruthenium-based catalysts, and HRP. The K_m value of the HRNs toward TMB (0.043 mM) was extremely small compared to those of other ruthenium catalysts and HRP, indicating a higher affinity to TMB. With

https://doi.org/10.1021/acsanm.3c01414
ACS Appl. Nano Mater. 2023, 6, 11435−11442

Table 1. Comparison of the Kinetic Parameters of the HRNs and Various Catalysts

catalyst	substrate	K_m (mM)	V_{max} $\times 10^{-8}$ (M s^{-1})	k_{cat} (s^{-1})	ref
HRP	TMB	0.434	10.00	4.00×10^3	2
	H_2O_2	3.70	8.71	3.48×10^3	
Ru frames	TMB	0.0603	13.4	1.26×10^4	42
	H_2O_2	318	7.41	6.98×10^3	
a-$RuTe_2$	TMB	0.419	39.1	1.12×10^1	43
	H_2O_2	18.4	83.9	2.40×10^1	
A-Ru	TMB	0.495	17.7		44
	H_2O_2	20.8	22.1		
HRN	TMB	0.043	24.3	1.00×10^5	this work
	H_2O_2	4.43	37.0	1.51×10^5	

H_2O_2, the HRNs had a K_m value of 4.43 mM, which was higher than that of HRP, indicating a lower affinity to H_2O_2 than HRP. However, the HRNs had a higher V_{max} (37.0×10^{-8} M s^{-1}) value than HRP (8.71×10^{-8} M s^{-1}), which indicated the ability of the HRNs to catalyze H_2O_2 more quickly. Moreover, the K_{cat} values of the HRNs toward TMB and H_2O_2 were much higher than those of HRP and other ruthenium catalysts, showing the higher catalytic efficacy of the HRNs. Figure 5E,F displays several Lineweaver−Burk plots at different concentrations of substrates. Each graph shows three lines intersecting at a point. These nonparallel lines indicate that the HRNs followed a sequential kinetic mechanism in which two substrates bind to the enzyme and form a ternary complex prior to release of the products.[36]

Catalytic Mechanism of the HRNs. Many previous reports have analyzed the catalytic mechanism of peroxidase-like nanozymes. The described mechanisms were based on generation of free radicals (e.g., •OH, O_2^-, h^+) or acceleration of electron transfer of substrates.[37−39] In general, the catalytic mechanism of peroxidase-like nanozymes was based on decomposition of H_2O_2 to the hydroxyl radical (•OH). To investigate this assumption, the generation of •OH was evaluated using TA, which easily reacts with •OH to produce a fluorescent product. As shown in Figure 6A, the presence of HRNs in the solution containing TA and H_2O_2 decreased the fluorescence of TA, suggesting that the HRNs reduced the production of •OH. In contrast, the strong fluorescence of TA was observed in the solution containing H_2O_2 and HRP, because the H_2O_2 was decomposed to •OH by HRP.[40] Consequently, the peroxidase-like activity of the HRNs was not based on generation of •OH.

In the next experiment, the catalytic mechanism of the HRNs was further investigated by monitoring the absorbance of TMB_{ox} in the presence of free radical scavengers (Figure 6B). In the reaction, DMSO, SOD, and EDTA were used as the scavengers for •OH, O_2^-, and h^+, respectively. The presence of scavengers showed negligible quenching effects for TMB oxidation, suggesting that the peroxidase-like activity of the HRNs does not originate from the generation of free radicals. Therefore, it is expected that the catalytic mechanism of the HRNs originated from the acceleration of electron transfer rather than free radical production. Previously, it was determined that the catalytic mechanism of Ru nanoparticles was based on facilitation of electron transfer between substrates and H_2O_2.[41] Thus, it was likely that TMB and H_2O_2 were adsorbed onto the HRNs, and TMB donated its lone-pair electrons to the HRNs. Then, the electrons were transferred from HRNs to H_2O_2, facilitating the oxidation of TMB.

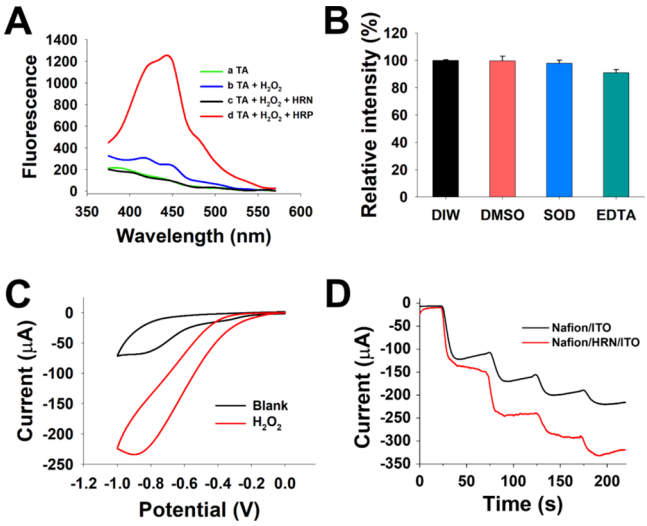

Figure 6. (A) Fluorescence spectra of TA with different compositions. (B) Effects of the radical scavengers toward the peroxidase-like activity of the HRNs. (C) CV of the Nafion/HRN/ITO electrode in the absence and presence of H_2O_2. Scan rate = 50 mV/s. (D) Amperometric responses of electrodes for the continuous addition of 1 M H_2O_2. Potential was fixed at −0.85 V.

To investigate the accelerated electron transfer, the electrochemical experiment for H_2O_2 redox reaction was performed. For analysis, ITO glass modified with Nafion and HRN (Nafion/HRN/ITO) was used as a working electrode. The CV showed obvious reduction response at around −0.85 V in the presence of H_2O_2 (Figure 6C). Based on this result, CA was conducted at a fixed potential of −0.85 V. As shown in Figure 6D, the current response of the Nafion/HRN/ITO electrode to the continuous addition of H_2O_2 was higher than that of the Nafion/ITO electrode. This result revealed that electron transfer between the electrode (electron donor) and H_2O_2 (electron acceptor) was facilitated by HRN.

Detection of CRP Using ELISA. The HRNs were applied to a conventional sandwich ELISA to detect CRP (Figure 7A). For the sandwich ELISA, the microplate was immobilized with cAb-CRP. Then, CRP was added to the microplate followed by the addition of dAb-HRNs. As the sandwich immunoreaction proceeded, each well had different concentrations of dAb-HRNs. The substrate solution (TMB and H_2O_2) was added and incubated. Finally, H_2SO_4 was added to quench the catalytic reaction, generating a yellow color (Figure 7B). The absorbance of the quenched reaction was measured at 450 nm. The HRN-based ELISA showed a linear relationship for CRP concentrations of 0.12−7.8 ng/mL (Figure 7C). In addition,

https://doi.org/10.1021/acsanm.3c01414
ACS Appl. Nano Mater. 2023, 6, 11435−11442

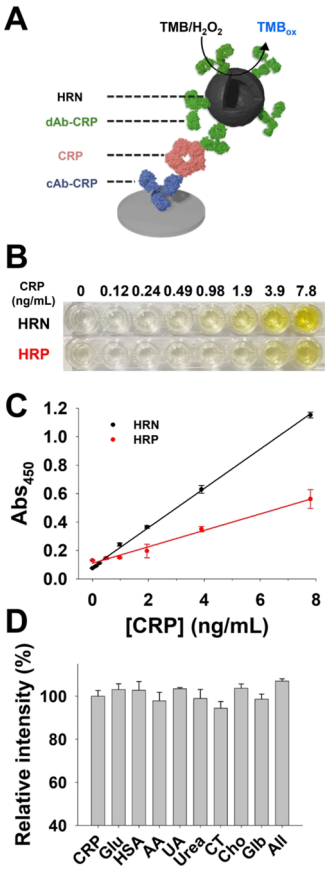

Figure 7. (A) Schematic illustration of HRN-based ELISA. (B) Photographs of HRN- and HRP-based ELISA. (C) Calibration curves. (D) Interference test for CRP detection using HRN-based ELISA. CRP level was fixed at 7.8 ng/mL. Concentration of interfering substances: HSA (50 mg/mL), glucose (1 mg/mL), AA (6 μg/mL), urea (200 μg/mL), UA (80 μg/mL), CT (12 μg/mL), Cho (5 mM), and Glb (20 mg/mL).

the limit of detection (LOD) of 33.2 pg/mL was obtained by using the standard formula of $3\sigma/s$, where σ represents the standard deviation of the blank samples, and s is the slope of the calibration curve. In contrast, conventional ELISA using HRP had a linear detection range of 0.49−7.8 ng/mL and the LOD of 0.27 ng/mL. Compared to HRP-based ELISA, the HRN-based ELISA showed better sensitivity in terms of detection range and LOD. This high sensitivity of HRN-based ELISA was attributed to the presence of hollow structure in nanoparticles, which increases the surface area and catalytic efficiency.

Moreover, the effects of interference on the HRN-based ELISA were investigated. The interfering factors were 1 mg/mL of Glu, 50 mg/mL of HSA, 6 μg/mL of AA, 80 μg/mL of UA, 200 μg/mL of urea, 12 μg/mL of CT, 5 mM of Cho, and 20 mg/mL of Glb. The concentration of interfering factors was determined based on normal levels in human serum. The absorbance signal of CRP concentration (7.8 ng/mL) in the presence of each interfering substance was measured using HRN-based ELISA. As shown in Figure 7D, the presence of interference had a negligible difference less than 10% compared to a standard solution that contained only CRP samples. This result revealed the high specificity of the HRN-based ELISA for the detection of CRP.

Recovery Test. To evaluate the validity of the HRN-based ELISA in real sample analysis, CRP samples (3 and 5 ng/mL) were spiked in human serum. Table 2 indicates the recovery of the CRP obtained by HRN-based ELISA. The recovery values of 3 and 5 ng/mL CRP in human serum were 97.0 and 98.4% with standard deviations of 2.94 and 2.28%, respectively. These results demonstrate that HRN-based ELISA can be utilized for the accurate determination of CRP in real samples.

Table 2. Determination of CRP in Human Serum Samples with HRN-Based ELISA

sample	added (ng/mL)	detected (ng/mL)	recovery (%)	RSD (%)
1	3.00	2.91	97.0	2.94
2	5.00	4.92	98.4	2.28

CONCLUSIONS

In the present study, HRNs were synthesized by a simple GRR. The hollow structure was generated using Ni NPs as a sacrificial template. The presence of the hollow structure increased the surface to volume ratio and facilitated a transfer of reactants. The HRNs presented in this work showed excellent peroxidase-like activity. The HRNs revealed comparable or superior catalytic efficiency to other ruthenium-based catalysts and HRP. Moreover, the HRNs followed a sequential kinetic mechanism. Further systematic studies revealed that the catalytic mechanism of the HRNs was based on enhanced electron transfer between the HRNs and substrates. The HRNs were applied to a conventional sandwich ELISA to detect the CRP. The HRN-based ELISA showed highly sensitive detection of CRP with good linearity from 0.12 to 7.8 ng/mL and the LOD of 33 pg/mL, which was more sensitive than HRP-based ELISA. In a recovery test, the HRN-based ELISA accurately detected CRP from spiked human serum, suggesting that the HRNs could be used as a probe to detect CRP in real samples. Based on these results, we believe that HRNs have numerous advantages, including facile preparation, low cost, and excellent catalytic efficiency, and can replace natural enzymes in a variety of fields.

ASSOCIATED CONTENT

Supporting Information

The Supporting Information is available free of charge at https://pubs.acs.org/doi/10.1021/acsanm.3c01414.

Michaelis−Menten equation; Lineweaver−Burk equation; turnover number; TEM images of the HRNs; XRD result of the HRNs; peroxidase-like activity of Ni NPs, Ru NPs, and HRNs (PDF)

AUTHOR INFORMATION

Corresponding Author

Gi Hun Seong − *Department of Bionano Engineering, Center for Bionano Intelligence Education and Research, Hanyang University, Ansan 426-791, Republic of Korea;* orcid.org/0000-0003-4688-713X; Phone: +82-31-400-5202; Email: ghseong@hanyang.ac.kr

Authors

Seong Eun Son − *Department of Bionano Engineering, Center for Bionano Intelligence Education and Research, Hanyang University, Ansan 426-791, Republic of Korea;* orcid.org/0000-0003-2293-3576

https://doi.org/10.1021/acsanm.3c01414
ACS Appl. Nano Mater. 2023, 6, 11435−11442

Pramod K. Gupta − *Department of Bionano Engineering, Center for Bionano Intelligence Education and Research, Hanyang University, Ansan 426-791, Republic of Korea*

Won Hur − *Department of Bionano Engineering, Center for Bionano Intelligence Education and Research, Hanyang University, Ansan 426-791, Republic of Korea;* orcid.org/0000-0002-4092-0165

Han Been Lee − *Department of Bionano Engineering, Center for Bionano Intelligence Education and Research, Hanyang University, Ansan 426-791, Republic of Korea*

Do Kyoung Han − *Division of Materials Analysis and Research, Korea Basic Science Institute, Daejeon 34133, Republic of Korea*

Complete contact information is available at: https://pubs.acs.org/10.1021/acsanm.3c01414

Notes

The authors declare no competing financial interest.

■ ACKNOWLEDGMENTS

This research was supported by the Basic Science Research Program through the National Research Foundation (NRF) of South Korea (2018R1A6A1A03024231 and 2021R1A2C1003566).

■ REFERENCES

(1) Liang, M. M.; Yan, X. Y. Nanozymes: From New Concepts, Mechanisms, and Standards to Applications. *Acc. Chem. Res.* **2019**, *52*, 2190−2200.

(2) Gao, L. Z.; Zhuang, J.; Nie, L.; Zhang, J. B.; Zhang, Y.; Gu, N.; Wang, T. H.; Feng, J.; Yang, D. L.; Perrett.; et al. Intrinsic peroxidase-like activity of ferromagnetic nanoparticles. *Nat. Nanotechnol.* **2007**, *2*, 577−583.

(3) Hayat, A.; Haider, W.; Raza, Y.; Marty, J. L. Colorimetric cholesterol sensor based on peroxidase like activity of zinc oxide nanoparticles incorporated carbon nanotubes. *Talanta* **2015**, *143*, 157−161.

(4) Wang, Z. Z.; Shen, X. M.; Gao, X. F.; Zhao, Y. L. Simultaneous enzyme mimicking and chemical reduction mechanisms for nanoceria as a bio-antioxidant: a catalytic model bridging computations and experiments for nanozymes. *Nanoscale* **2019**, *11*, 13289−13299.

(5) He, L.; Li, Y.; Wu, Q.; Wang, D. M.; Li, C. M.; Huang, C. Z.; Li, Y. F. Ru(III)-Based Metal-Organic Gels: Intrinsic Horseradish and NADH Peroxidase-Mimicking Nanozyme. *ACS Appl. Mater. Interfaces* **2019**, *11*, 29158−29166.

(6) Li, W.; Bin, C.; Zhang, H. X.; Sun, Y. H.; Wang, J.; Zhang, J. L.; Fu, Y. BSA-stabilized Pt nanozyme for peroxidase mimetics and its application on colorimetric detection of mercury(II) ions. *Biosens. Bioelectron.* **2015**, *66*, 251−258.

(7) Gao, Z.; Wang, C.; He, J.; Chen, P. Pd@Pt Nanodendrites as Peroxidase Nanomimics for Enhanced Colorimetric ELISA of Cytokines with Femtomolar Sensitivity. *Chemosensors* **2022**, *10*, 359.

(8) Lou-Franco, J.; Zhao, Y.; Nelis, J. L. D.; Stewart, L.; Rafferty, K.; Elliott, C.; Cao, C. Smartphone-based immunochemical sensor exploiting peroxidase-like activity of ligand-capped gold nanostars: A proof-of-concept detection of Mycobacterium bovis. *Biosens. Bioelectron.* **2023**, *220*, No. 114857.

(9) Nicklen, F. D.; Diaz, A. J.; Lu, J.; Patel, S. T.; Zheng, E. M.; Campbell, V. R.; Wu, B. M.; Kamei, D. T. Application of the aqueous two-phase system and nanozyme signal enhancement for the improved detection of Plasmodium lactate dehydrogenase in serum. *Anal. Bioanal. Chem.* **2022**, *414*, 7949−7956.

(10) Lou, Z. P.; Zhao, S.; Wang, Q.; Wei, H. N-Doped Carbon As Peroxidase-Like Nanozymes for Total Antioxidant Capacity Assay. *Anal. Chem.* **2019**, *91*, 15267−15274.

(11) Wu, L.; Yan, H.; Li, G. H.; Xu, X.; Zhu, L.; Chen, X. Q.; Wang, J. Surface-Imprinted Gold Nanoparticle-Based Surface-Enhanced Raman Scattering for Sensitive and Specific Detection of Patulin in Food Samples. *Food Anal. Method* **2019**, *12*, 1648−1657.

(12) Gupta, P. K.; Son, S. E.; Seong, G. H. One-pot synthesized citric acid-modified bimetallic PtNi hollow nanospheres as peroxidase mimics for colorimetric detection of human serum albumin. *Mater. Sci. Eng., C* **2020**, *116*, No. 111231.

(13) Son, S. E.; Gupta, P. K.; Hur, W.; Lee, H. B.; Park, Y.; Park, J.; Kim, S. N.; Seong, G. H. Citric Acid-Functionalized Rhodium-Platinum Nanoparticles as Peroxidase Mimics for Determination of Cholesterol. *ACS Appl. Nano Mater.* **2021**, *4*, 8282−8291.

(14) Park, Y.; Gupta, P. K.; Tran, V. K.; Son, S. E.; Hur, W.; Lee, H. B.; Park, J. Y.; Kim, S. N.; Seong, G. H. PVP-stabilized PtRu nanozymes with peroxidase-like activity and its application for colorimetric and fluorometric glucose detection. *Colloids Surf., B* **2021**, *204*, No. 111783.

(15) Lou-Franco, J.; Das, B.; Elliott, C.; Cao, C. Gold Nanozymes: From Concept to Biomedical Applications. *Nano-Micro Lett.* **2021**, *13*, 10.

(16) Das, B.; Franco, J. L.; Logan, N.; Balasubramanian, P.; Kim, M. I.; Cao, C. Nanozymes in Point-of-Care Diagnosis: An Emerging Futuristic Approach for Biosensing. *Nano-Micro Lett.* **2021**, *13*, 193.

(17) Ren, X.; Chen, D.; Wang, Y.; Li, H.; Zhang, Y.; Chen, H.; Li, X.; Huo, M. Nanozymes-recent development and biomedical applications. *J. Nanobiotechnol.* **2022**, *20*, 92.

(18) Su, D. N.; Zhang, X. M.; Wu, A. P.; Yan, H. J.; Liu, Z. Y.; Wang, L.; Tian, C. G.; Fu, H. G. CoO-Mo_2N hollow heterostructure for high-efficiency electrocatalytic hydrogen evolution reaction. *NPG Asia Mater.* **2019**, *11*, 78.

(19) Wang, X. J.; Feng, J.; Bai, Y. C.; Zhang, Q.; Yin, Y. D. Synthesis, Properties, and Applications of Hollow Micro-/Nanostructures. *Chem. Rev.* **2016**, *116*, 10983−11060.

(20) Xue, C.; Zhou, X.; Li, X.; Yang, N.; Xin, X.; Wang, Y.; Zhang, W.; Wu, J.; Liu, W.; Huo, F. Rational Synthesis and Regulation of Hollow Structural Materials for Electrocatalytic Nitrogen Reduction Reaction. *Adv. Sci.* **2022**, *9*, No. e2104183.

(21) Zhao, M.; Xu, L.; Vara, M.; Elnabawy, A. O.; Gilroy, K. D.; Hood, Z. D.; Zhou, S.; Figueroa-Cosme, L.; Chi, M. F.; Mavrikakis.; et al. Synthesis of Ru Icosahedral Nanocages with a Face-Centered-Cubic Structure and Evaluation of Their Catalytic Properties. *ACS Catal.* **2018**, *8*, 6948−6960.

(22) Xu, J. Q.; Chen, Z.; Ren, D. F.; Xiang, X. C.; Chen, N.; Li, X. F.; Ye, Z. X.; Chen, Q. M.; Ma, S. Y. Preparation of hollow nanoparticles with controllable diameter by one-step controlled etching of microporous silica particles using an ammonia-based etchant. *Colloids Surf., A* **2020**, *592*, No. 124579.

(23) Kim, J. W.; Choi, S. H.; Lillehei, P. T.; Chu, S. H.; King, G. C.; Watt, G. D. Cobalt oxide hollow nanoparticles derived by bio-templating. *Chem. Commun.* **2005**, *32*, 4101−4103.

(24) Wang, H. F.; Lin, G. H.; Li, X. Q.; Lu, W. S.; Peng, Z. C. Self-standing hollow porous AuPt nanospheres and their enhanced electrocatalytic performance. *J. Colloid Interface Sci.* **2019**, *554*, 396−403.

(25) Chen, Z. L.; Zhang, J. F.; Zhang, Y.; Liu, Y. W.; Han, X. P.; Zhong, C.; Hu, W. B.; Deng, Y. D. NiO-induced synthesis of PdNi bimetallic hollow nanocrystals with enhanced electrocatalytic activities toward ethanol and formic acid oxidation. *Nano Energy* **2017**, *42*, 353−362.

(26) Zhang, W. Q.; Yang, J. Z.; Lu, X. M. Tailoring Galvanic Replacement Reaction for the Preparation of Pt/Ag Bimetallic Hollow Nanostructures with Controlled Number of Voids. *ACS Nano* **2012**, *6*, 7397−7405.

(27) Cobley, C. M.; Xia, Y. N. Engineering the properties of metal nanostructures via galvanic replacement reactions. *Mater. Sci. Eng., R* **2010**, *70*, 44−62.

(28) da Silva, A. G. M.; Rodrigues, T. S.; Haigh, S. J.; Camargo, P. H. C. Galvanic replacement reaction: recent developments for

engineering metal nanostructures towards catalytic applications. *Chem. Commun.* **2017**, *53*, 7135−7148.
(29) Kang, Y. S.; Jung, J. Y.; Choi, D.; Sohn, Y.; Lee, S. H.; Lee, K. S.; Kim, N. D.; Kim, P.; Yoo, S. J. Formation Mechanism and Gram-Scale Production of PtNi Hollow Nanoparticles for Oxygen Electrocatalysis through In Situ Galvanic Displacement Reaction. *ACS Appl. Mater. Interfaces* **2020**, *12*, 16286−16297.
(30) Ghosh, S.; Singh, P.; Roy, S.; Bhardwaj, K.; Jaiswal, A. Superior Peroxidase-Like Activity of Gold Nanorattles in Ultrasensitive H_2O_2 Sensing and Antioxidant Screening. *ChemBioChem* **2022**, *23*, No. 202100691.
(31) Choi, N.; Dang, H.; Das, A.; Sim, M. S.; Chung, I. Y.; Choo, J. SERS biosensors for ultrasensitive detection of multiple biomarkers expressed in cancer cells. *Biosens. Bioelectron.* **2020**, *164*, No. 112326.
(32) Harris, D. C. *Quantitative Chemical Analysis*; W. H. Freeman, 2010.
(33) Wang, P.; Zong, L. L.; Guan, Z. J.; Li, Q. Y.; Yang, J. J. PtNi Alloy Cocatalyst Modification of Eosin Y-Sensitized g-C_3N_4/GO Hybrid for Efficient Visible-Light Photocatalytic Hydrogen Evolution. *Nanoscale Res. Lett.* **2018**, *13*, 33.
(34) Guo, L. L.; Mao, L.; Huang, K. X.; Liu, H. M. Pt-Se nanostructures with oxidase-like activity and their application in a selective colorimetric assay for mercury(II). *J. Mater. Sci.* **2017**, *52*, 10738−10750.
(35) Laage, D.; Elsaesser, T.; Hynes, J. T. Water Dynamics in the Hydration Shells of Biomolecules. *Chem. Rev.* **2017**, *117*, 10694−10725.
(36) Stefanidis, L.; Scinto, K. V.; Strada, M. I.; Alper, B. J. Bisubstrate Kinetics of Glutathione S-Transferase: A Colorimetric Experiment for the Introductory Biochemistry Laboratory. *J. Chem. Educ.* **2018**, *95*, 146−151.
(37) Wei, J. P.; Chen, X. L.; Shi, S. G.; Mo, S. G.; Zheng, N. F. An investigation of the mimetic enzyme activity of two-dimensional Pd-based nanostructures. *Nanoscale* **2015**, *7*, 19018−19026.
(38) Cui, M. L.; Zhou, J. D.; Zhao, Y.; Song, Q. J. Facile synthesis of iridium nanoparticles with superior peroxidase-like activity for colorimetric determination of H_2O_2 and xanthine. *Sens. Actuators, B* **2017**, *243*, 203−210.
(39) Song, Y. J.; Qu, K. G.; Zhao, C.; Ren, J. S.; Qu, X. G. Graphene Oxide: Intrinsic Peroxidase Catalytic Activity and Its Application to Glucose Detection. *Adv. Mater.* **2010**, *22*, 2206−2210.
(40) Miura, T. A mechanistic study of the formation of hydroxyl radicals induced by horseradish peroxidase with NADH. *J. Biochem.* **2012**, *152*, 199−206.
(41) Cao, G. J.; Jiang, X.; Zhang, H.; Croley, T. R.; Yin, J. J. Mimicking horseradish peroxidase and oxidase using ruthenium nanomaterials. *RSC Adv.* **2017**, *7*, 52210−52217.
(42) Ye, H. H.; Mohar, J.; Wang, Q. X.; Catalano, M.; Kim, M. J.; Xia, X. H. Peroxidase-like properties of Ruthenium nanoframes. *Sci. Bull.* **2016**, *61*, 1739−1745.
(43) Yan, H. Y.; Chen, Y. F.; Jiao, L.; Gu, W. L.; Zhu, C. Z. Amorphous $RuTe_2$ nanorods as efficient peroxidase mimics for colorimetric immunoassay. *Sens. Actuators, B* **2021**, *341*, No. 130007.
(44) Tang, Y. J.; Wu, Y.; Xu, W. Q.; Jiao, L.; Chen, Y. F.; Sha, M.; Ye, H. R.; Gu, W. L.; Zhu, C. Z. Ultrathin Ruthenium Nanosheets with Crystallinity-Modulated Peroxidase-like Activity for Protein Discrimination. *Anal. Chem.* **2022**, *94*, 1022−1028.

https://doi.org/10.1021/acsanm.3c01414
ACS Appl. Nano Mater. 2023, 6, 11435−11442